NEYART
Magazine
ISSN: 2992 - 7161

CHARACTERIZATION AND DESIGN OF A SOLAR OVEN USING TONATIUH TO ANALYZE BREAD BAKING EFFICIENCY

CHARACTERIZATION AND DESIGN OF A SOLAR OVEN USING TONATIUH TO EVALUATE BAKING EFFICIENCY

Verdugo-Urías José Bulmaro, National Technological Institute of Mexico/I.T. de Los Mochis https://orcid.org/0009-0007-6178-3722
jose.vu@tecnm.mochis.mx

Argüeso-Mendoza, Yeniba
National Technological Institute of Mexico/Los Mochis Institute of Technology
https://orcid.org/0000-0002-5691-7841
yeniba.am@mochis.tecnm.mx

Ochoa-Espinoza Valente
National Technological Institute of Mexico/Los Mochis Institute of Technology
https://orcid.org/0009-0005-6163-962X
valente.oe@mochis.tecnm.mx

Miranda-Arnold Juan Andrés
National Technological Institute of Mexico/Los Mochis Institute of Technology
https://orcid.org/0009-0003-7597-4248
juan.ma@mochis.tecnm.mx

Ruiz-Ibarra Jesús Iván
National Technological Institute of Mexico/Los Mochis Institute of Technology https://orcid.org/0000-0001-8800-9314
jesus.ri@mochis.tecnm.mx

DOI: https://doi.org/10.61273/neyart.v4i1.206 **Received: 02/19/2026** | **Accepted:** 04/25/2026 | **Published:** 05/27/2026

Abstract—This project focuses on the characterization and design of a solar furnace that uses a parabolic dish as a concentrator, with specifications of 70 cm in diameter, 61.25 cm focal length, and 5 cm depth. The tests included the design of a flat heliostat with a solar tracker (configured as a square with side-by-side dimensions) and the estimation of the radiant flux distribution and the maximum power obtained on a circular target 20 cm in diameter located at the focal length. A parametric analysis was conducted to evaluate how the position of the target relative to the focal length (slant range), the size of the receiver (diameter), the zenith angle, and the reflectivity percentage of the concentrator affect the furnace's efficiency in terms of power (watts), as well as the maximum power obtained during the four seasons (solstices or equinoxes) of the year 2024. Tests were also conducted without a heliostat to analyze the effect of direct solar radiation on the oven's design. The results indicate that the maximum power on the 20-cm-diameter target is 312 Watts with a heliostat and 332 Watts without a heliostat. The estimates were calculated using the open-source ray-tracing software "Tonatiuh."
Keywords—Bread baking, solar energy, solar oven, Tonatiuh software.

Abstract-- This project focuses on the characterization and design of a solar oven that uses a satellite dish as a concentrator, with specifications of 70 cm in diameter, 61.25 cm in focal length, and 5 cm in depth. The tests included the design of a planar heliostat with a solar tracker (configured as a square with dimensions Side × Side) and the estimation of the radiant flux distribution and the maximum power obtained on a circular target 20 cm in diameter located at the focal distance. A parametric analysis was performed to evaluate how the position of the target relative to the focal length (slant range), the size of the receiver (diameter), the zenith angle, and the reflectivity percentage of the concentrator affect the oven's efficiency in terms of power (watts), as well as the maximum power obtained during the four seasons (solstices and equinoxes) of the year 2024. Tests were also conducted without a heliostat to analyze the effect of direct solar radiation on the furnace design. The results indicate that the maximum power on the 20-cm-diameter target is 312 Watts with the heliostat and 332 Watts without it. The estimates were made using the open-source ray-tracing software "Tonatiuh."

Keywords: Bread baking, solar energy, solar oven, Tonatiuh software.

INTRODUCTION

Solar ovens are simple devices that harness solar energy for cooking food (Solar Gastronomy, 2023), (Roulet, 2010). The search for sustainable and efficient alternatives for cooking food has been a topic of growing interest in the field of scientific and technological research (Esteves et al., 2006), (González et al., 2014), (Del Río et al., 2010). In this context, solar ovens emerge as a promising option that not only reduces dependence on fossil fuels but also contributes to mitigating environmental impact. This thesis project aims to characterize and design a solar oven using the Tonatiuh software, focusing on analyzing efficiency in terms of power during the bread-baking process.

This research also promotes the development of clean and accessible technologies, contributing to Goal 7 of the Sustainable Development Goals (SDGs) (Affordable and Clean Energy) (UN, 2018). This comprehensive approach has the potential to propose an alternative to the pita bread baking process currently carried out at a pizzeria located in Los Mochis, Sinaloa, Mexico—which uses LP gas—by designing a solar oven that meets the thermal needs of the process through technological innovation in the field of clean energy, in this case, solar energy.

The human activity that has the greatest impact on the global ecological footprint is the food production system; in other words, the way we produce what we eat is rapidly degrading our planet, accounting for 70% of biodiversity loss on land and 50% in freshwater, and is responsible for approximately 30% of greenhouse gas emissions (World Wildlife Fund, 2022). Furthermore, according to the Economic Commission for Latin America and the Caribbean (ECLAC), the world's population is growing rapidly, reaching a total of 8 billion people in 2021—a population four times larger than the world's population in 1927; the 2022 revision of the United Nations' population estimates and projections forecasts that the population will reach 9 billion in 15 years and 10 billion by 2058 (ECLAC, 2022).

DEVELOPMENT

Methodology

This study was carried out in two main stages: ray tracing simulation using the Tonatiuh software and the processing of the data generated by the software, including the creation of graphs, curve fitting, and analysis of the variables involved and their respective indicators using the software's flow analysis feature, all within a framework based on the following studies: (Marín, 2017), (Flores et al., 2021), (Sánchez, 2016).

Tonatiuh software

Tonatiuh uses the Monte Carlo method to calculate flow maps and optical efficiencies in solar thermal systems, making it particularly well-suited for complex structures and heliostat fields. It is free software that allows users to access and modify the code, fostering collaboration and continuous development; Tonatiuh includes a graphics library that allows users to create both simple and complex three-dimensional geometries, facilitating the modeling of different surfaces and structures; Specific applications of the software include: modeling and simulating a parabolic trough collector—one of the technologies used in solar thermal energy systems—and simulating a heliostat field (mirrors that track the sun's path) to concentrate solar radiation onto a receiver; The software offers (once the entire system is in place), prior to simulation, a flow analysis that includes information such as incident flow distribution, maximum power, maximum flow, average flow, minimum flow, error, and uniformity; It is also capable of outputting binary and SQL files containing information on the photons on the surface to be studied (CENER, 2017), (Blanco, 2018).

1. Initial Software Parameters

Tonatiuh uses a series of input parameters to define how solar radiation is distributed in space and time within the simulation. These parameters include aspects such as the optical, geometric, and energetic distribution of the solar source. The correct selection and adjustment of the input parameters in Tonatiuh are essential to ensure that the simulation accurately reflects the behavior of the real solar system (Canales, 2022).

1.1 Solar Shape

Among its features, Tonatiuh offers two solar shapes that can be used to simulate solar radiation in different applications; for this research, the Buie shape was used (it is considered the closest to the Sun's actual shape) (Flores et al., 2021) with a circum-solar ratio (CSR) of 0.02 and an irradiance of 1000 W/m². Figure 1 shows the selection of the initial solar shape parameter in the Tonatiuh software.

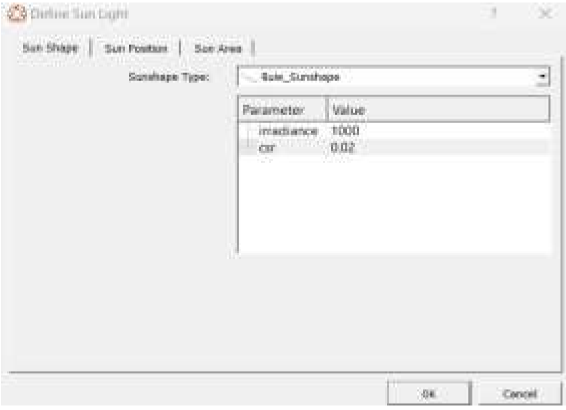

Figure 1. *Initial parameter for the solar shape selected in the simulation.*

Note: *The Buie solar shape and an irradiance of 1000 $^{W/m^2}$ were set.*

Source: *Author's own work.*

1.2 Solar Position

This parameter varies depending on the time of observation of the solar system and depends on two angles: the azimuth and the elevation (relative to the horizon), both measured in degrees. For the purposes of this study, an elevation angle of 90° and an azimuth angle of 0° were considered. Figure 2 shows the solar position parameters described above in the software.

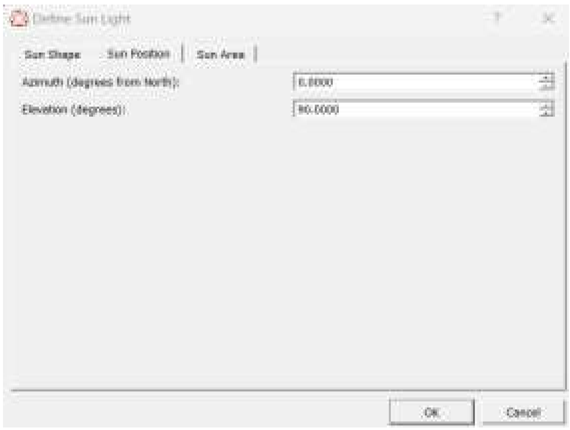

Figure 2. *Definition of the parameters: azimuth and elevation angles in the software.*

Note: *Both angle configurations are shown: azimuth of 0° and elevation of 90°.*

Source: *Author's own work.*

1.3 Optical Quality

This parameter is measured using the optical error, which encompasses the various errors associated with a normal deviation in the reflective system—in this case, the heliostat and the receiver. Tonatiuh assigns and groups all optical errors—including those caused by the non-uniform angular distribution of sunlight, slope error from the concentrator, specularity error, aiming error, and others related to tracking and sensors—using the sigma slope parameter; its unit of measurement is mrad (Flores et al., 2021). A standard value for the error in parabolic dish systems is 6.7 mrad, according to Stine and Greyer (2001), cited in (Flores et al., 2021). Equation 1a determines the total optical error of a solar furnace.

$$\sigma^2 = \sigma^2_{sol} + \sigma^2_{pen} + \sigma^2_{espe} + \sigma^2_{pun} \quad \text{Eq. (1)}$$

Where:

σ^2 = Total optical error

σ^2_{sol} = Error caused by the non-uniform angular distribution of the sun's rays

σ^2_{pen} = Concentrator slope error

σ^2_{espe} = Specularity error

σ^2_{pun} = Aiming error (the receiver is not positioned exactly at the focal point)

As a starting point, the optical error of the concentrator, heliostat, and receiver surfaces will be set to the software's default value of 3 milliradians (Figure 3); subsequently, we will evaluate the impact on the solar furnace's efficiency using values of 1.5 and 7 mrad.

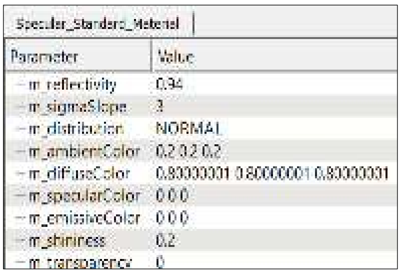
Specular_Standard_Material

Parameter	Value
m_reflectivity	0.94
m_sigmaSlope	3
m_distribution	NORMAL
m_ambientColor	0.2 0.2 0.2
m_diffuseColor	0.80000001 0.80000001 0.80000001
m_specularColor	0 0 0
m_emissiveColor	0 0 0
m_shininess	0.2
m_transparency	0

Figure 3. *Estimation of optical error (sigma slope).*

Note: *The configuration shown corresponds to an optical error of 3 mrad. All other settings remain at their default values.*

Source*: Author's own work.*

2. Simulation

NEYART
Magazine
ISSN: 2992 - 7161

Following the proposed methodology, we proceed to implement the numerical simulation of the solar system. The developed model considers four main components: a solar radiation source (previously defined in the initial parameters), a heliostat with a control system for solar tracking, a parabolic concentrator, and the receiver. The simulation will allow us to evaluate the furnace's efficiency in terms of power.

2.1 Geometry of the System Components

Tonatiuh offers a wide range of geometries for simulating each of the solar system's components; the most important are: cone, sphere, cylinder, rectangle, and parabolic disk (Figure 4). To generate each element, the software uses two types of nodes (Figure 5): the Group node, which is assigned to each element of the system and contains the element's position and spatial rotation attributes; and the Surface node, which is used to assign a geometry and corresponding attributes to each element—such as a parabolic disk to the concentrator, a rectangle to the heliostat, and a circle to the receiver; Within the surface nodes, the desired material is assigned via Specular_Standard_Material; each of the system's nodes and surfaces is shown in Figure 6.

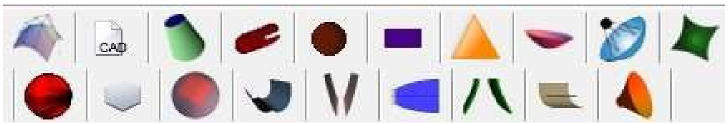

Figure 4. *Geometries available in Tonatiuh.*

Note: *For this study, we will use a parabolic disk, a flat plate, and a flat rectangle.*

Source*: Author's own work.*

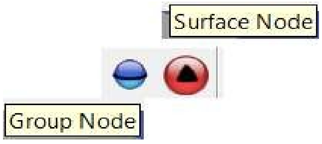

Figure 5. *Types of nodes***.**

Note: *Group and surface nodes. In this research project, only group nodes were used to assign the various elements and surfaces.*

Source: Author's *own work.*

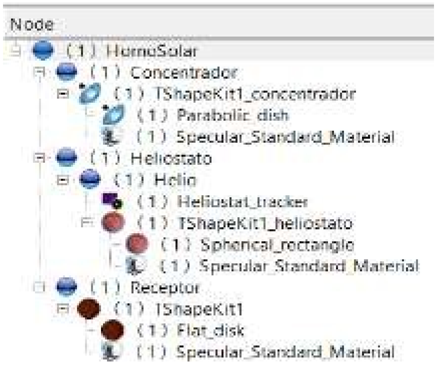

Figure 6. *Different nodes that make up the system, geometry, and materials.*

Note: *The figure shows the main node, corresponding to the solar furnace, and the subnodes associated with the system's components: concentrator, heliostat, and receiver.*

Source: *Author's own work.*

2.2 Characterization of the Elements

Once the main nodes, as well as the surface nodes and the geometric shapes of the elements, have been defined, the corresponding attributes for the concentrator, the heliostat, and the receiver of the solar system will be established.

2.2.1 Parabolic concentrator

It is located within the solar furnace node; the concentrator's specifications are as follows:

Table 1. *Specifications of the parabolic concentrator.*

Parámetro	Medición	
	Centímetros	Conversión (m)
Diámetro	70 cm	.70 m
Profundidad	5cm	0.05 m
Distancia focal	61.25 cm	.6125 m

Note: *The parameters of diameter, depth, and focal length are shown.*
Source: *Author's own work.*

The *position* attributes (rotation of 90 degrees relative to the horizontal corresponding to $\frac{\pi}{2}$ *rad* = 1.5708); *geometry* (focal length 0.6125 m, minimum radius 0 m, maximum radius 0.35 m); and *material* (reflectivity percentage of 94%, optical error of 3 mrad) were captured at the node corresponding to the concentrator and are shown in Figure 7; the other attributes retain their default values.

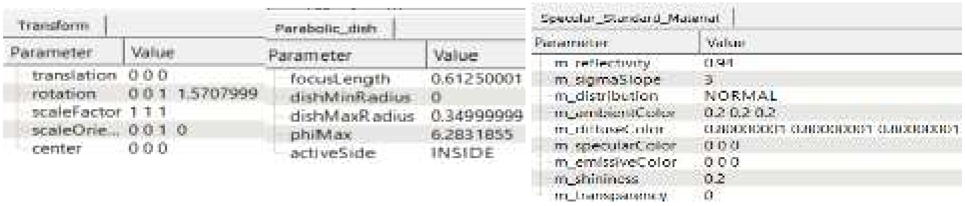

Figure 7. *Concentrator parameters.*

Note: *The attributes related to the optimal values for the concentrator are shown; these are: position, geometry, and reflectivity percentage.*

Source: *Author's own work.*

2.2.2 Heliostat

The heliostat has a square geometry, with dimensions of 1.4 meters per side (Equations 2 and 3). It is located 1.84 m from the concentrator. The reflective material, which is shaped like a flat rectangle, has a reflectivity of 94%.

$$L = D + 2 \cdot d \cdot Tan\left(\frac{\theta}{2}\right) \qquad \text{Eq. (2)}$$

$$Tan\left(\frac{\theta}{2}\right) = \frac{D}{2F} \qquad \text{Eq. (3)}$$

Where:
L = Side of the heliostat
D = Diameter of the concentrator
F and d = Focal length of the concentrator

To perform the heliostat simulation, it is essential to set up a main node (Heliostat) that contains the position and rotation attributes. Next, a surface-type node (Helio) must be added that includes a heliostat tracker; this configuration allows for the simulation of the heliostat's automatic orientation adjustment based on the sun's position. Figure 8 shows the attributes required for the heliostat simulation.

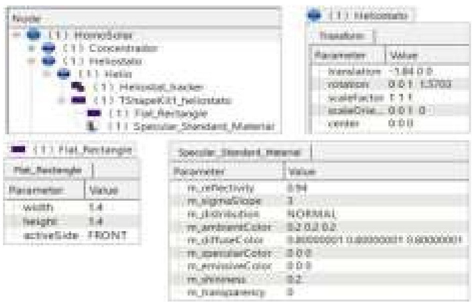

Figure 8. *Nodes for the heliostat in the simulator and various design and optical parameters*.

Note: *Attributes related to the heliostat are shown: geometric shape, measurement parameters, reflectivity, distance from the concentrator, and optical error.*
Source: *Author's own work.*

2.2.3 Receiver

The receiver is located at the focal distance of the concentrator (0.6125 meters); its geometric shape is a flat disk with a diameter of 20 cm, which corresponds approximately to the size of the bread to be baked; this is where all the energy will be concentrated.

To model the receiver in the simulator, a main node named "Receiver" is added to the solar oven node, where its position and rotation are defined. Within this main node, a surface node named "Plate" is inserted; it is assigned the geometry of a flat disk (flat_disk) and specified as a specular material with a reflectivity of 0% in order to maximize the absorption of solar radiation. The receiver's attributes are illustrated in Figure 9.

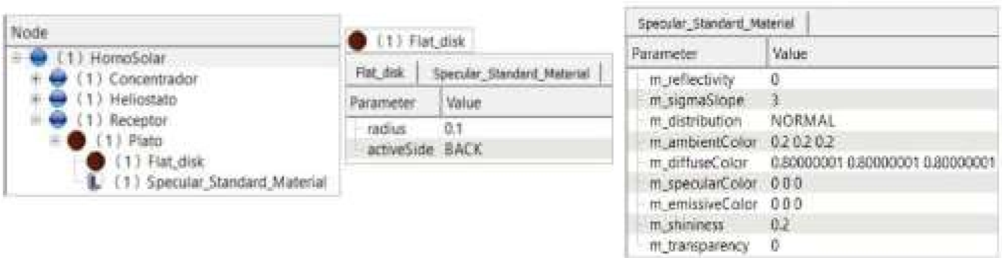

Figure 9. *Characterization of the receiver, design and optical attributes.*

Note: *The attributes related to the receiver are shown: geometric shape, design parameters (radius), reflectivity, and optical error.*

Source: *Author's own work*

Figure 10 shows a detailed graphical representation of the final design of the solar furnace system in the Tonatiuh software, in which all of its components can be seen.

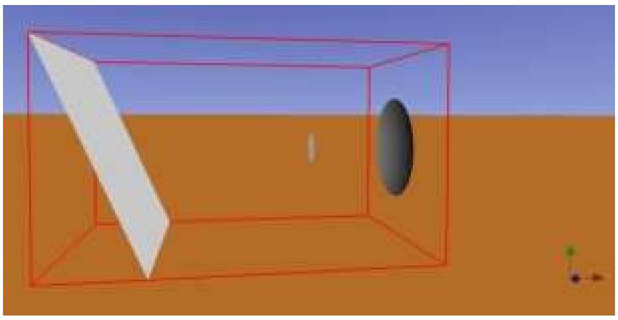

Figure 10. *Final design of the solar oven in the Tonatiuh software, front view.*

Note: *Shown from left to right are the heliostat, the receiver, and the solar concentrator.*

Source: *Author's own work.*

Figure 11 presents a simulation of the solar furnace system, in which 1,000 solar rays have been plotted to visualize their trajectories and evaluate the concentration efficiency.

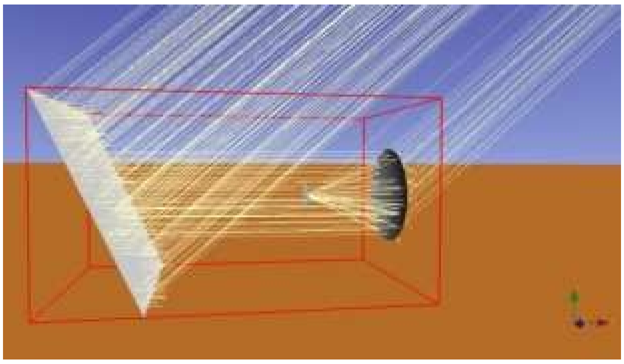

Figure 11. *Simulation with 1,000 rays.*

Note: *The front view of the solar system is shown with the incidence of 1,000 rays.*

Source: *Author's own work.*

Figure 12 shows all the nodes, which include the surface, geometry, and specular material of each element that makes up the solar furnace.

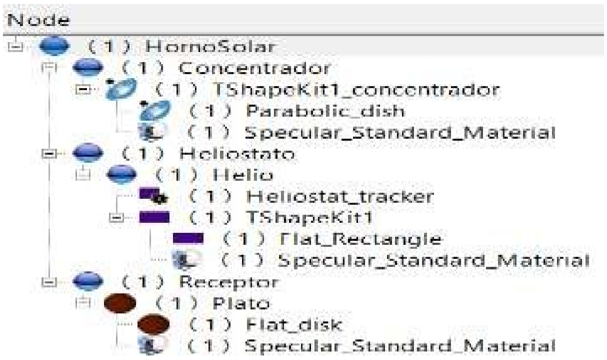

Figure 12. *Code window showing all the nodes that make up the solar system.*

Note: *The three elements that make up the solar oven are presented, grouped into nodes and subnodes according to the required elements.*

Source: *Author's own work*

2.3 Simulation and Execution Parameters

Once the system definition was complete, the simulation was carried out. First, the number of rays to be traced was determined, considering that a greater number of rays results in a reduction in the statistical error of the obtained results (Sánchez, 2016). The maximum number of rays the software can trace is 75 million; for this number of rays, the error is approximately 0.5% (Sánchez, 2016). To set the number of rays in the software, the following command sequence is used: Ray Trace menu / Ray Trace Options…; Figure 13 shows the settings window for defining the number of rays.

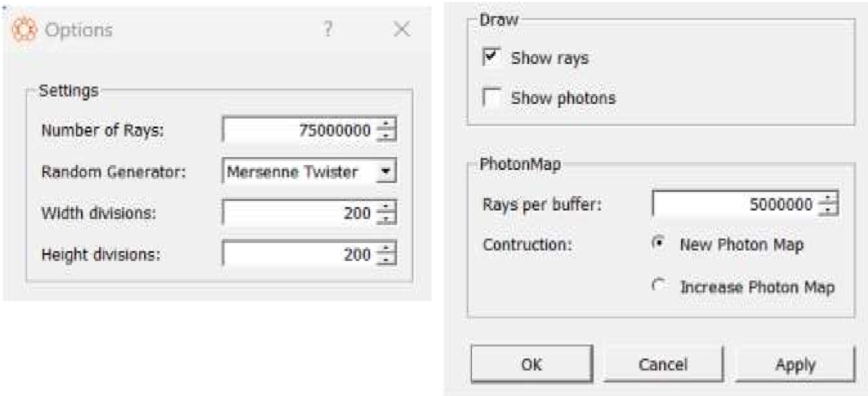

Figure 13. *Tonatiuh ray tracing options window.*

Note: *The configuration for the maximum number of rays and the activation of the "Show Rays" option in the simulation are shown.*

Source: *Author's own work.*

Once the number of rays has been selected, the simulation is run using the Ray Trace/Run command sequence. The software offers three options for storing data: SQL Database, Binary File, and Not

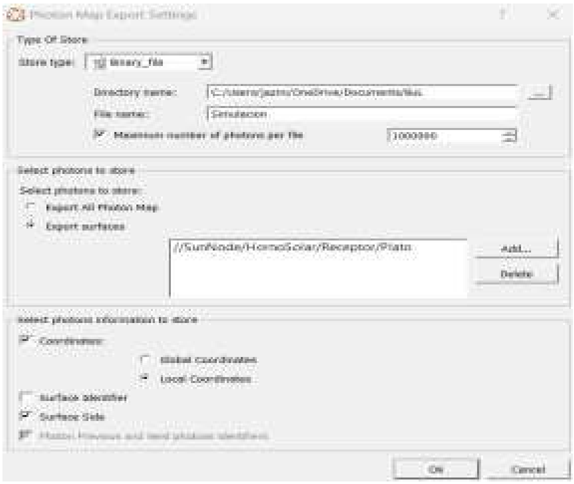

Figure 3. *Tonatiuh execution window for storing binary data*

Note: *The attributes required to run the simulation with the proposed design configuration are shown.*

Source: *Author's own work.*

Export. For the first two options, you must select a destination folder where the data will be saved, as well as the file name. Next, select the surface to be studied, which in this case is the receiver, where the solar rays from the concentrator strike at the defined focal length (Figure 14).

ANALYSIS OF RESULTS

Four hypotheses were proposed, which will be evaluated according to the proposed methodology and compared with the results obtained from the flux analysis performed using the Tonatiuh software, employing the maximum number of rays—75 million—for each analysis.

Analysis of Hypothesis 1

Ho: The optical error (Sigma Slope) assigned to the reflective material of the solar furnace components does not affect efficiency in terms of power.

The power of the solar furnace, with optical error or sigma slope values of 3 mrad—captured as an attribute on the surface of the material (Specular Standard Material)—in the three system components—heliostat, concentrator, and receiver—yields a power of 314.57 Watts. Figure 15 shows the results of the flux analysis with these parameters.

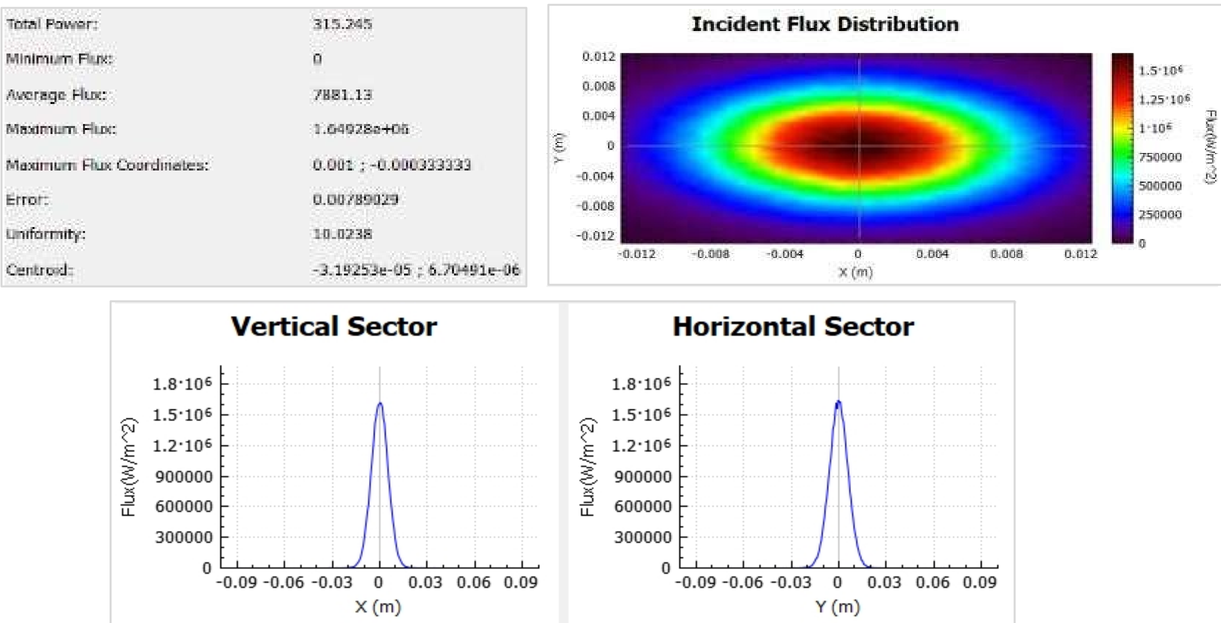

Figure 15. *Flux analysis for an optical error of 3 mrad and the power reflected at the rear of the receiver.*

Note: According to the data, the system power was 315.245 Watts, and the maximum incident flux on the receiver was 1.65MW/m². It can be observed that the incident flux, in both the vertical and horizontal sectors, reaches a maximum of 3 cm.

Source: *Author's own work.*

When the optical error is changed to 5 mrad on the surface of the materials of the three solar furnace elements, under the same conditions as in the previous analysis, the software calculates a power of 315.08 Watts at the receiver. Figure 16 shows the results of the flux analysis using these parameters.

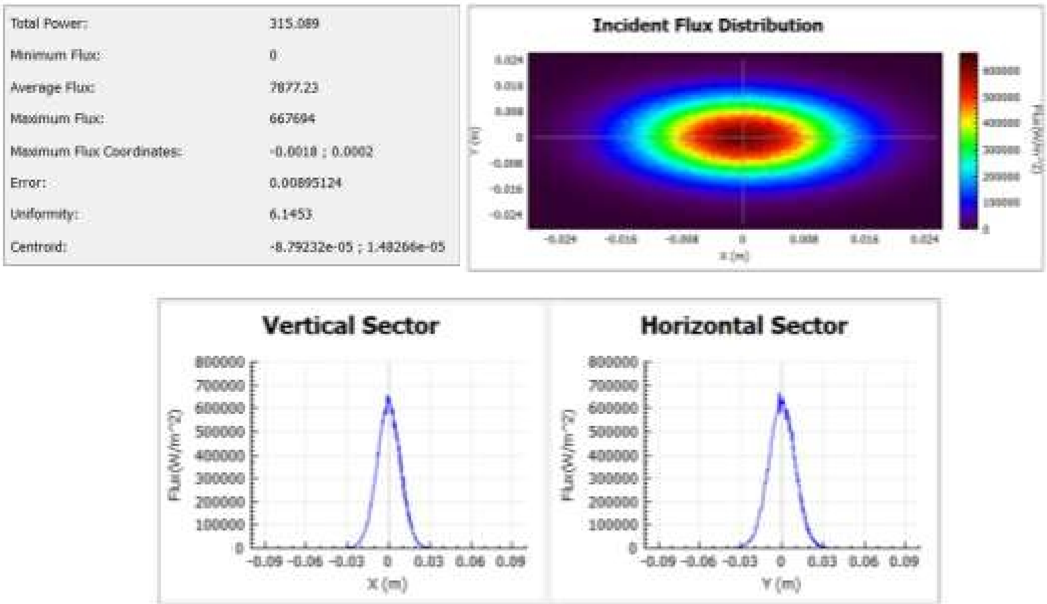

Figure 16. *Flux analysis for an optical error of 5 mrad and the power reflected at the rear of the receiver.*

Note: *According to the data, the system power was 315.089 Watts, and the maximum incident flux on the receiver was 0.667MW/m 2. It can be observed that the incident flux in both the vertical and horizontal sectors has a maximum range of 3 cm.*

Source: *Author's own work.*

Finally, when simulating an optical error of 7 mrad on the surface of the materials of the three solar furnace elements—under the same conditions as in the previous analysis—the software calculates a power of 315,141 Watts at the receiver. Figure 17 shows the results of the flux analysis using these parameters.

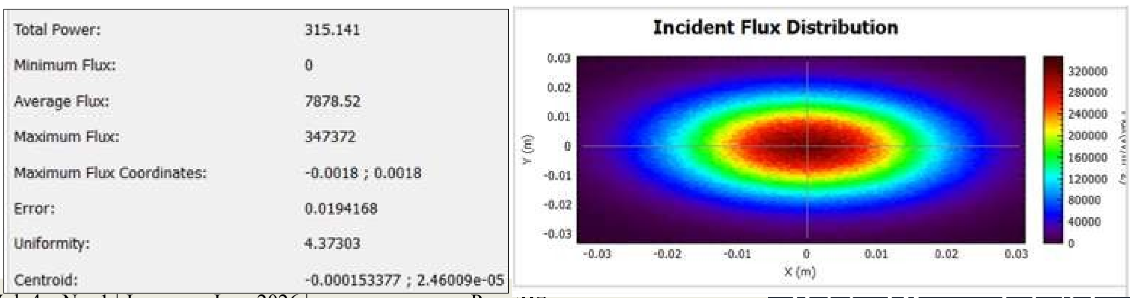

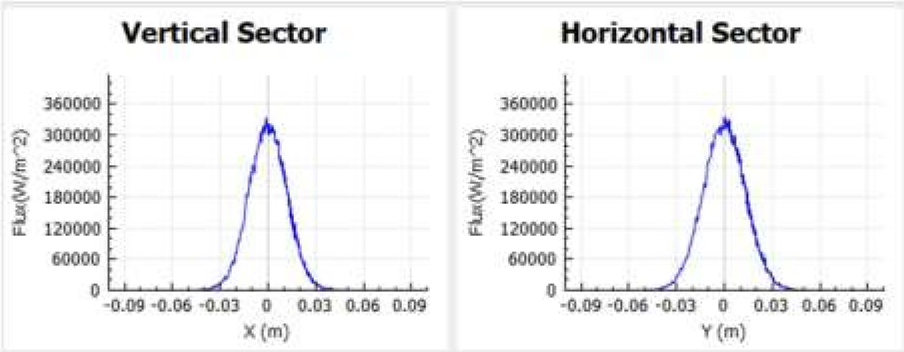

Figure 17. *Flux analysis for an optical error of 7 mrad and the power reflected at the rear of the receiver.*

Note*: According to the data, the system power was 315.141 Watts, and the maximum flux incident on the receiver was 0.347* MW/m^2*, and it can be seen that the incident flux in both the vertical and horizontal sectors has a maximum range of 3 cm.*

Source*: Author's own work.*

Analysis of Hypothesis 2

Ho: The focal distance (slant range) of the receiver relative to the solar concentrator does not affect the power efficiency of the solar furnace.

The influence of the receiver's position relative to the focal point (slant range) is analyzed, considering a range of $f = 0.6125m$, $\pm 0.15m$. In this analysis, the common parameters will be the optical error, set by default to 3 mrad, and the number of rays, set to 75 million. The position values,
sorted numerically, are as follows: 0.3125 m, 0.4625 m, 0.6125 m, 0.7625 m, and 0.9125 m.

Figure 18 shows the configuration of the fixed parameters: optical error (m_sigma) set to 3 mrad and the number of rays set to the maximum value possible for the simulator, 75 million.

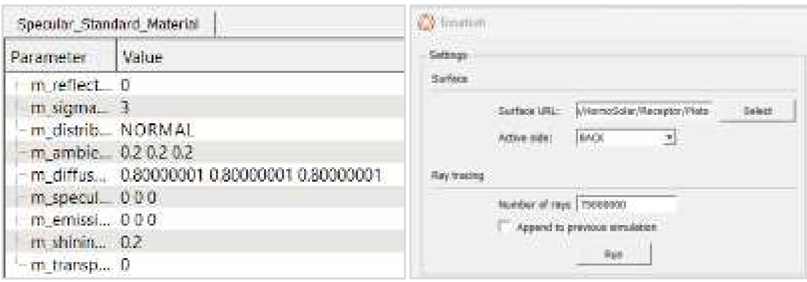

Figure 18. *Configuration parameters for analyzing different Slant Range values*

Note*: The maximum number of rays was adjusted, and the default value for optical error was maintained at 3 mrad for each element of the system.*

Source*: Author's own work.*

The flow analysis for each of the focal length variations (Slant Range) is shown below.

Figure 19 shows the flux analysis for a Slant Range of 0.3125 m.

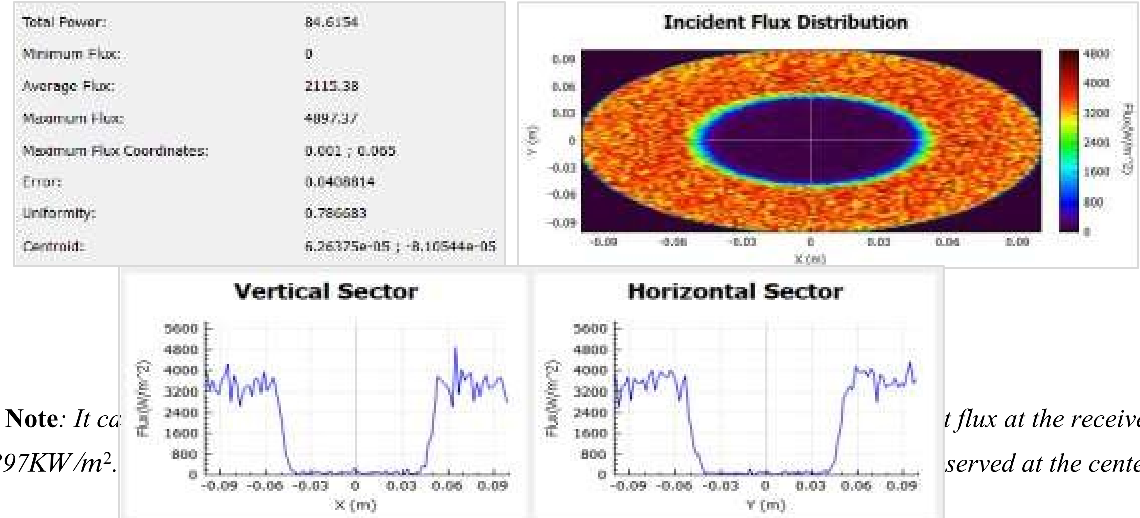

Note: *It ca… t flux at the receiver of 4.897KW/m². … served at the center of the receiver, caused by the change in the adjusted position.*

Source: *Author's own work.*

Figure 20 shows the flow analysis when the receiver is positioned at a slant range of 0.4625 m.

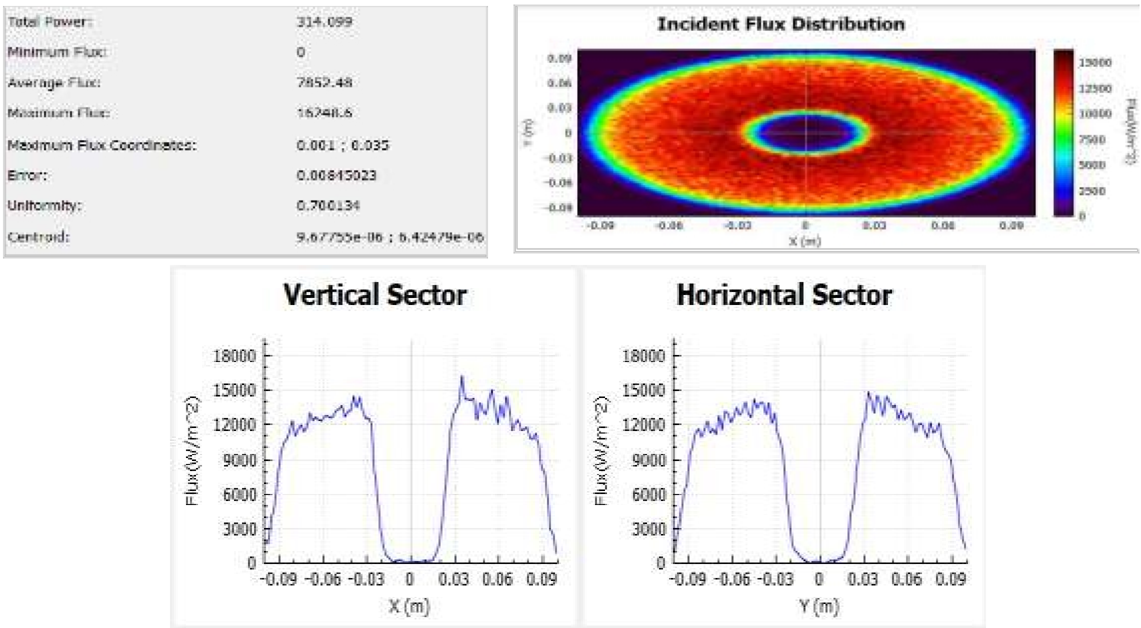

Figure 20. *Flow analysis for a slant range of 0.4625 m.*

Note: The system power was 314.099 Watts, and the maximum flow incident on the receiver was 16.248 KW/m ² was observed. In the vertical and horizontal sectors, a flow loss of approximately 2.8 cm is observed at the center of the receiver. Source: Author's own work.

Figure 21 shows the flow analysis when the receiver is positioned at a slant range of 0.6125 m.

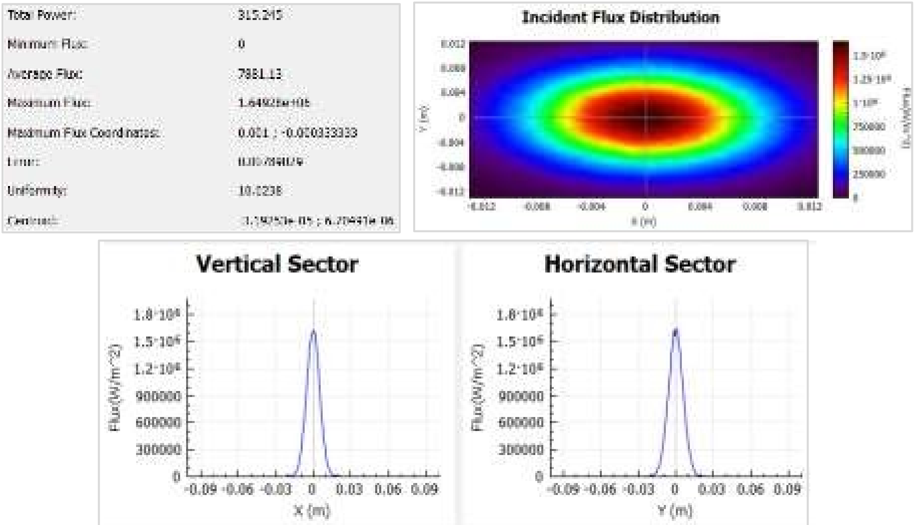

Figure 21. *Flow analysis for a slant range of 0.6125 m.*

Note*: The system power was 315.245 Watts, and the maximum incident flux on the receiver was 1.65 MW/m² . It can also be seen that the maximum incident flow is located at the center of the receiver and is lost above 3 cm.*

Source*: Author's own work.*

Figure 22 shows the flow analysis when the receiver is positioned at a slant range of 0.7625 m.

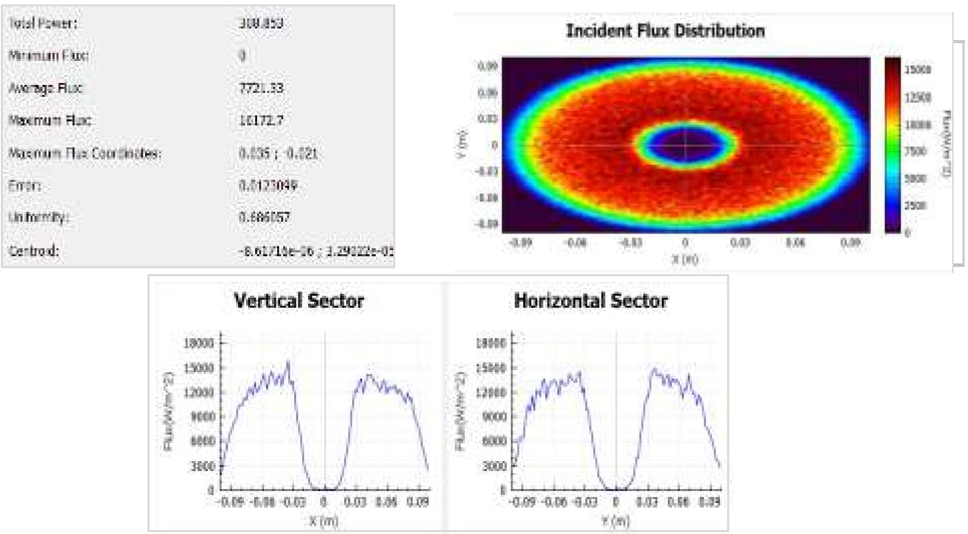

Figure 22. Flow analysis for a slant range of 0.7625 m

Note: *It can be seen that the system power was 308.853 Watts, and the maximum incident flux on the receiver was 16.172 KW/m^2 (2). In the vertical and horizontal sectors, a flow loss of approximately 3 cm is observed at the center of the receiver.*

Source: *Author's own work.*

Figure 23 shows the flow analysis when the receiver is positioned at a slant range of 0.9125 m.

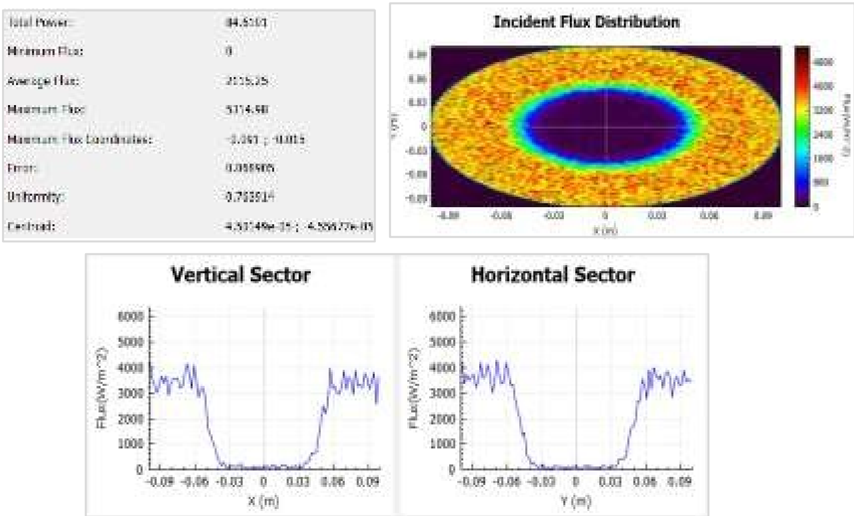

Figure 23. *Flow analysis for a slant range of 0.9125 m.*

Note: *The system power was 84.6101 Watts, and the maximum incident flux on the receiver was 5.314 KW/m^2 (2). In the vertical and horizontal sectors, a flow loss of approximately 5 cm is observed at the center of the receiver.*

Source: *Author's own work*

Figure 24 below summarizes the slant range configurations considered in this study for the receiver and the solar concentrator.

Figure 24. *Different positions or Slant Ranges*.

Note: *The Slant Range positions of 0.3125 m, 0.4625 m, 0.6125 m, 0.7625 m, and 0.9125 m are shown in order from left to right.*

Source: *Compiled by the author*

Analysis of Hypothesis 3

Ho: The use of a heliostat at a certain distance from the solar concentrator does not affect the furnace's efficiency in terms of power.

The optimal efficiency of the solar furnace is determined under the following conditions: an optical error of 3 mrad, a focal length of 0.6125 m, and a reflectivity of 94% on both the concentrator's surface and the heliostat's surface. The heliostat measures 1.4 m on each side and is located 1.84 m away from the concentrator.

In addition, the heliostat is equipped with a solar tracking system that allows it to continuously reflect the sun's rays toward the concentrator, regardless of the azimuth and elevation angles of the sun at the time of testing. Figure 20 (Flux Analysis for a Slant Range of 0.6125 m) presents the complete flux analysis, in which the power output by the simulator was 315.245 Watts and the

of 1.65MW/m^2 .

To perform a comparative analysis of the solar furnace without using the heliostat, it was necessary to adjust the rotation parameters of the concentrator and the receiver, as well as the solar position. It was decided to position the solar concentrator facing upward (Figure 25), placing the receiver at a focal length of 0.6125 m. As for the solar position, an elevation angle of 90° was set, allowing the sun's rays to strike the concentrator directly and be reflected toward the receiver.

In this case, the direct solar radiation preset in the software—equivalent to 1000 W/m²—was used. Figure 25 presents the flux analysis under the described conditions.

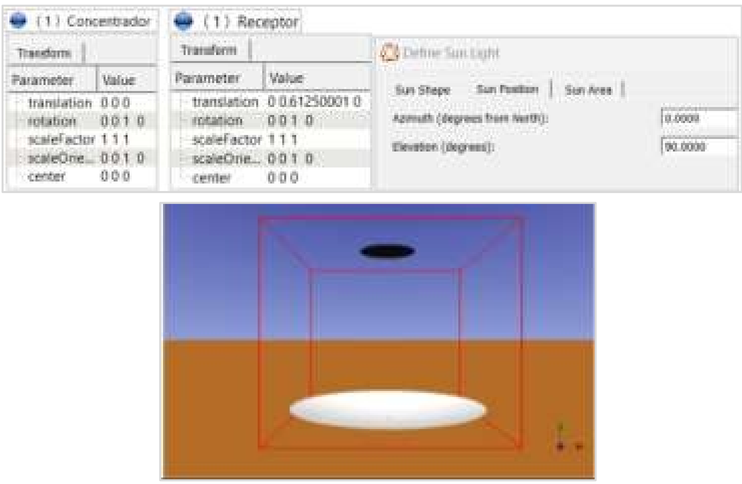

Figure 25. *Position of the concentrator and receiver.*

NEYART
Magazine
ISSN: 2992 - 7161

Note: *Both the concentrator and the receiver have a value of 0 radians in the fourth coordinate (0, 0, 1, 0), which orients them upward. It should be noted that the receiver's translation parameter along the y-axis is 0.6125 (0, 0.6125, 0), which allows it to be positioned at the focal length. Additionally, the solar position attributes established prior to the simulation are included.*

Source*: Author's own work*

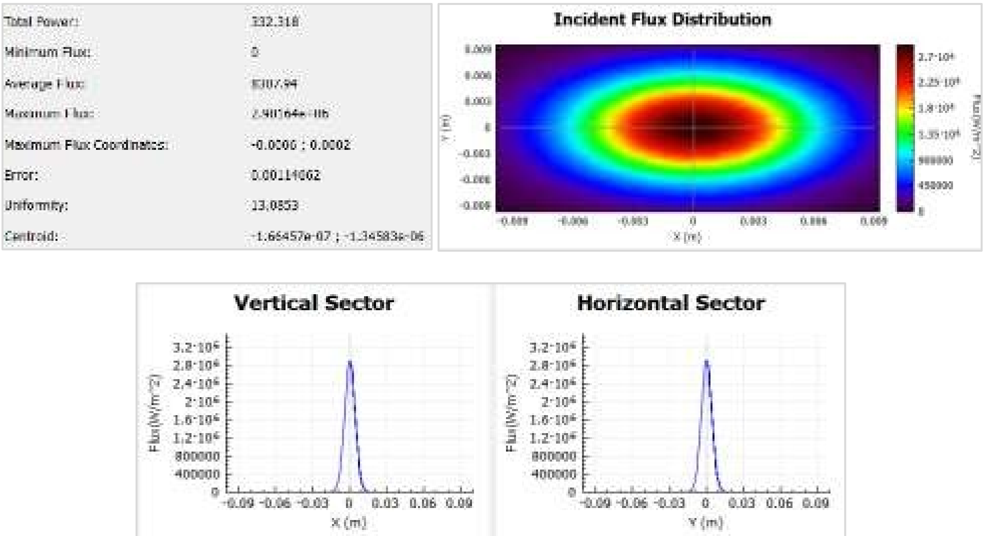

Figure 26. *Flux analysis without the use of the heliostat (direct solar radiation).*

Note: *The system power was 332.318 Watts, and the maximum incident flux on the receiver was 2.9 MW/m*^{2}*. It can also be seen that the maximum incident flux is at the center of the receiver and is lost above 1.5 cm.*

Source*: Author's own work.*

Analysis of Hypothesis 4

Ho: Changing the receiver's radius does not affect the solar furnace's efficiency in terms of power.

The influence of variations in the receiver's design parameters—specifically its radius—is analyzed, considering a range of $r = 0.1m \pm 0.02\ m$. The simulation parameters established for each case are: an optical error of 3 mrad and a total of 75 million rays. The

of flux includes the three elements—the heliostat and the concentrator—configured with the initial design, optical, and positioning parameters. The different values for the receiver radius, listed numerically, are as follows: 0.06 m, 0.08 m, 0.1 m, 0.12 m, and 0.14 m.

Figure 27 shows the flux analysis obtained by setting the receiver radius to 0.06 m.

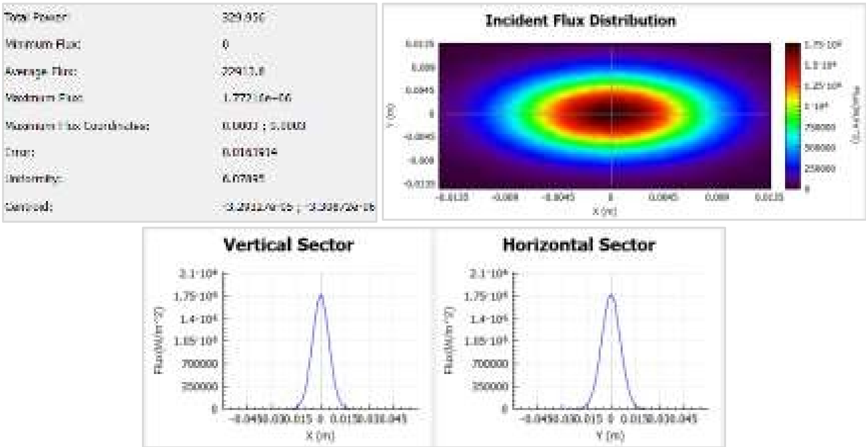

Figure 27. *Flux analysis at the receiver with a radius of 0.06 m.*

Note: *It can be seen that the system power was 329.956 Watts, and the maximum incident flux at the receiver was 1.77 MW/m² . It can also be seen that the maximum incident flux is located at the center of the receiver and is lost above 1.5 cm.*

Source*: Author's own work.*

Figure 28 presents the flow analysis obtained by setting a radius of 0.08 m for the receiver.

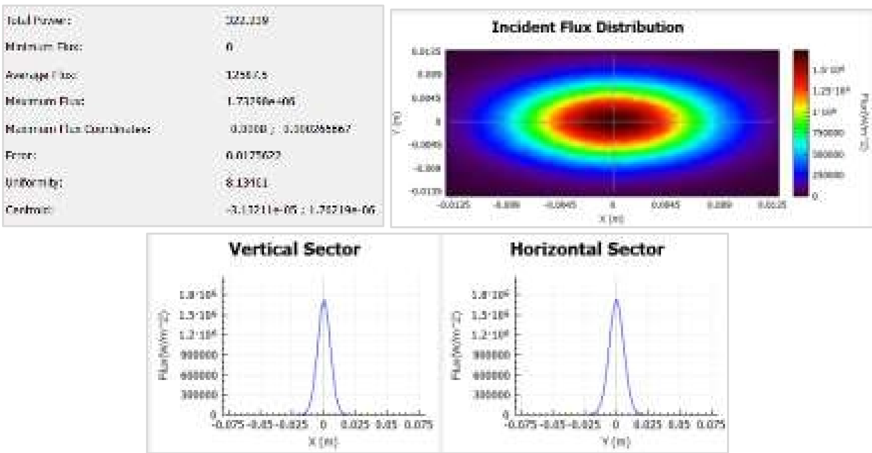

Figure 28. *Flow analysis at the receiver with a radius of 0.08 m.*

Note*: It can be seen that the system power was 322.239 Watts, and the maximum incident flux on the receiver was 1.73 MW/m² . It can also be seen that the maximum incident flux is located at the center of the receiver and is lost above 1.25 cm.*

Source*: Author's own work.*

Figure 29 presents the flow analysis obtained by setting a radius of 0.1 m for the receiver.

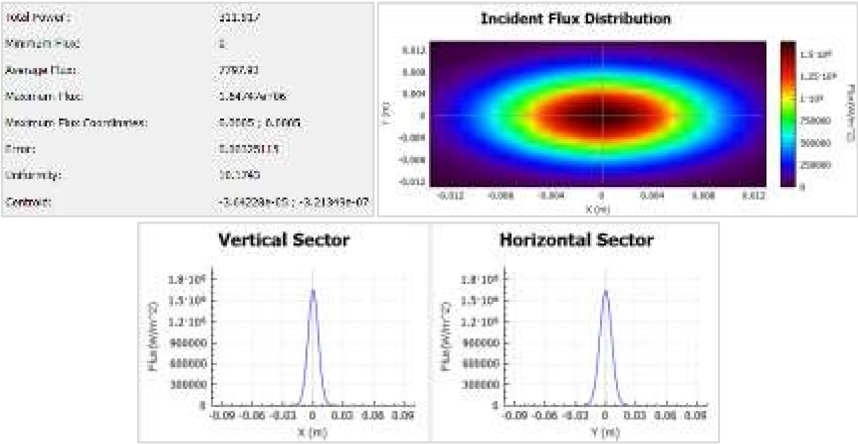

Figure 29. *Flow analysis in the receiver with a radius of 0.1 m.*

Note: *The system power was 311.91 Watts, and the maximum incident flux on the receiver was 1.64 MW/m² . It can also be seen that the maximum incident flux is located at the center of the receiver and is lost above 1.5 cm.*

Source*: Author's own work.*

Figure 30 presents the flow analysis obtained by setting the receiver radius to 0.12 m.

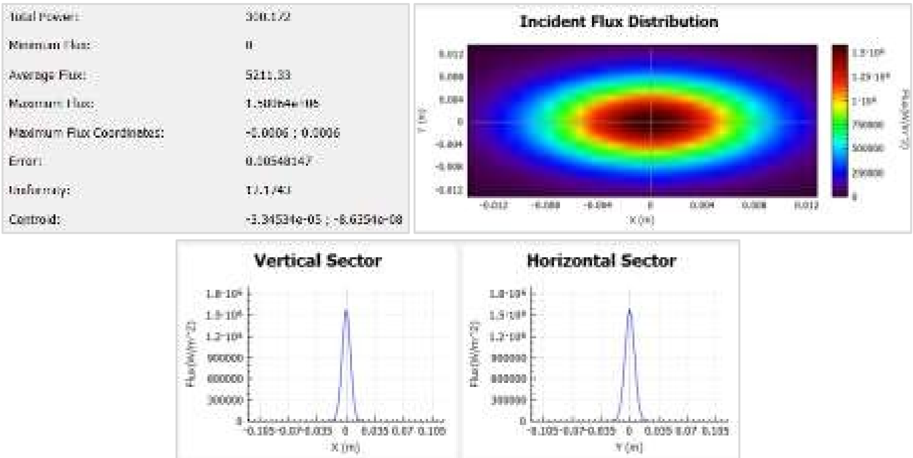

Figure 30. *Flow analysis in the receiver with a radius of 0.12 m.*

Note: *It can be seen that the system power was 300.172 Watts, and the maximum incident flux on the receiver was 1.58 MW/m² . It can also be seen that the maximum incident flux is located at the center of the receiver and is lost above 2.1 cm.*

Source*: Prepared by the author.*

Finally, Figure 31 shows the flow analysis obtained by setting a radius of 0.14 m in the receiver.

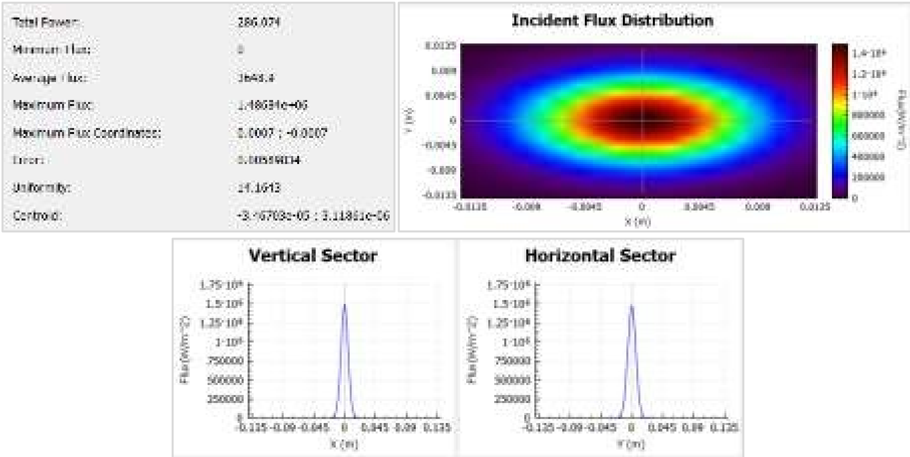

Figure 31. *Flow analysis at the receiver with a radius of 0.14 m.*

Note: *It can be seen that the system power was 286.074 Watts, and the maximum flux incident on the receiver was 1.48 MW/m*^{2} *. It can also be seen that the maximum incident flux is located at the center of the receiver and is lost above 1.5 cm.*

Source: *Author's own work.*

CONCLUSIONS

Based on the results obtained through the flux analysis provided by the software, it was determined that the *optical error* variable (*Sigma Slope*) does not significantly affect the efficiency of the solar furnace. The power generated in the receiver remained constant, at around **315 Watts**, with minimal variations, even in the face of changes in the values of this variable. Therefore, it is concluded that the *optical error* does not significantly influence the system's power.

The flux analysis for the *Slant Range* variable shows that it significantly influences the efficiency of the solar oven. At very short distances (0.3125 m) or very long distances (0.9125 m), the power drops dramatically to **84.6 Watts**. In contrast, at the focal length proposed in the design (0.6125 m), maximum power—**315.245 Watts**—is achieved, establishing this as the optimal distance. These results demonstrate that the proposed design meets the required efficiency criteria.

When analyzing the variable related to the use of the heliostat in the solar system, the flux analysis reveals a slight difference in the power generated at the receiver.

Specifically, when the heliostat is present, the power reached is **315.245 Watts**, whereas, in its absence, the power generated amounts to **332.318 Watts**. This occurs because the effect of the cumulative reflection generated by the heliostat's reflective surface is omitted. When the system includes all its components, the rays undergo two reflections (at the heliostat and at the concentrator) before reaching the receiver, resulting in cumulative losses. These losses are calculated as the product

of the reflectivity factors of both surfaces, that is, $\rho_t = (\rho_h)(\rho_c)$ (Sosa, 2015).

In the case analyzed, both surfaces have a reflectivity factor of 0.94, resulting in a total loss due to reflection of $0.94 \, x \, 0.94 = 0.8836$.

Finally, the flux analysis for the receiver radius variable reveals a decrease in the power

generated as the radius increases. At a radius of 0.06 m, the power reaches **329.956 Watts**, while increasing the radius to 0.14 m reduces the generated power to **286.074 Watts**.

Future Work

Although all the hypotheses proposed were analyzed and tested satisfactorily, certain recommendations were identified based on the simulation:

- Examine variations in the *Sigma Slope* or critical optical errors that may influence the power output of the solar furnace. This will allow for the establishment of an optimal range of minimum and maximum values suitable for the specific proposed design.
- After analyzing the effect of *the Slant Range* on the design, it is recommended to make smaller variations based on the initially proposed focal length. This will allow for the identification of the critical minimum values of distance (moving farther away or closer) that affect efficiency.
- Conduct an oversizing test of the heliostat to evaluate its impact on efficiency, as well as tests involving moving the heliostat farther away or closer in relation to the focal length.

Consider identifying an optimal point for radius sizing in the proposed solar system design, even if that value does not exactly match the project's specific requirements.

References

Blanco, M. (2018). Tonatiuh: An object-oriented, distributed computing, Monte Carlo ray tracer for the design and simulation of solar concentrating systems. *University of Texas at Brownsville*, (pp. 1–

2).
https://www.researchgate.net/publication/237256255_Tonatiuh_An_object_oriented_distributed_computing_Monte-Carlo_ray_tracer_for_the_design_and_simulation_of_solar_concentrating_systems

Canales, B. (2022). CHARACTERIZATION OF SOLAR CONCENTRATION GEOMETRIES USING MODELS OF TRACING RAY RAY *University of Chile*. https://repositorio.uchile.cl/handle/2250/186634

CENER. (2017). *Tonatiuh.* https://github.com/iat-cener/tonatiuh

ECLAC. (2022). The world's population reaches 8 billion, of whom 662 million live in Latin America and the Caribbean. *United Nations*. https://www.cepal.org/es/noticias/mundo-alcanza-8-mil-millones-habitantes-cuales-662-millones-viven-america-latina-caribe

Del Río, J., Tapia, S., and Jaramillo, O. (2010). Solar cookers. *Digital University Journal. Energy Research Center—National Autonomous University of Mexico, Vol. 11* (No. 10), p. 4. https://www.revista.unam.mx/vol.11/num10/art93/art93.pdf

Esteves, A., Buenanueva, F., and Cavagnaro, L. (2006). *PASTEURIZATION OF MILK USING A SOLAR* (Vol. 10). (A. e. Environment, Ed.) Argentina: ASADES. https://ri.conicet.gov.ar/bitstream/handle/11336/40499/CONICET_Digital_Nro.f941ff90-f645-4f62-9320-827b800b311b_A.pdf?sequence=2&isAllowed=y

Flores, V., Sánchez, M., Bedolla, J., and Bedolla, H. (2021). Concentration and distribution of solar radiation at the receiver of a parabolic dish concentrator. *PROCEEDINGS OF THE 27TH INTERNATIONAL ANNUAL OF THE SOMIM.* https://somim.org.mx/memorias/memorias2021/articulos/A4_37.pdf

Solar Gastronomy. (2023). *Solar Oven.* Spain. https://gastronomiasolar.com/horno-solar/

González, M., López, L., Servín, H., and González, D. (2014). *STUDY OF THE THERMAL PROPERTIES OF THE TOLOKATZIN SOLAR OVEN.* Juriquilla, Querétaro, Mexico: PROCEEDINGS OF THE 20TH INTERNATIONAL ANNUAL ON THE SOMIM.
https://www.researchgate.net/publication/317078518_ESTUDIO_DE_PROPIEDADES_TERMICASE_STUDY_OF_THE_TOLOKATZIN_SOLAR_OVEN

Marín, J. (2017). Study on the Implementation and Modeling of a Small Solar Oven in Tonatiuh. *University of Seville*. https://biblus.us.es/bibing/proyectos/abreproy/91100/fichero/TFG+JLMG.pdf

UNITED NATIONS. (2018). *The 2030 Agenda and the Sustainable Development Goals: An Opportunity for Latin America and the Caribbean.* United Nations, Santiago: United Nations Publication. https://repositorio.cepal.org/server/api/core/bitstreams/cb30a4de-7d87-4e79-8e7a-ad5279038718/content

Roulet, E. (2010). Solar Cooking. *FROM PATAGONIA: SHARING KNOWLEDGE, Vol. 7*(No. 10). https://desdelapatagonia.uncoma.edu.ar/wp-content/uploads/2019/01/4.-Revista-N10_Roulet.pdf

Sánchez, F. (2016). Design and Analysis of a Small Solar Oven Using Tonatiuh. *University of Seville*. https://idus.us.es/server/api/core/bitstreams/b924edfb-f798-49d6-ae89-5174f6f7ce2c/content Sosa, P. (2015). DEVELOPMENT OF A METHODOLOGY FOR THE DESIGN AND CHARACTERIZATION OF AN AXIS-CENTERED SOLAR FURNACE WITH THERMAL CAPACITY OF 1KW. *UNIVERSITY OF SONORA. DIVISION OF ENGINEERING*. https://concentracionsolar.org.mx/images/pdf/tesis/m2_pablo_sosa_corregida.pdf

World Wildlife Fund. (2022). Living Planet Report 2022: Toward a Society in Positive Harmony with Nature. *Almond*, pp. 67–69. https://wwflpr.awsassets.panda.org/downloads/descarga_informe_planeta_vivo_2022_1_1_1.pdf

Collaborative Work Table

Role	Author(s)
Research	José Bulmaro Verdugo Urías, Yeniba Argüeso Mendoza
Data Curation	Yeniba Argüeso Mendoza, Valente Ochoa Espinoza
Writing - Preparation of the original draft	José Bulmaro Verdugo Urías, Yeniba Argüeso Mendoza
Writing—Review and Editing	Jesús Iván Ruiz Ibarra, Yeniba Argüeso Mendoza
Visualization	Jesús Iván Ruiz Ibarra, Yeniba Argüeso Mendoza

Supervision	Juan Andrés Miranda Arnold, Valente Ochoa Espinoza